Biosensors and Bioelectronics 107 (2018) 26–33

Contents lists available at ScienceDirect

Biosensors and Bioelectronics

journal homepage: www.elsevier.com/locate/bios

Development of a molecularly imprinted polymer tailored on disposable screen-printed electrodes for dual detection of EGFR and VEGF using nano-liposomal amplification strategy

Mohammad Johari-Ahar[a], Pari Karami[a], Mostafa Ghanei[b], Abbas Afkhami[c], Hasan Bagheri[b,*]

[a] Department of Bioanalytical Sciences and Medicinal Chemistry, School of Pharmacy, Ardabil University of Medical Sciences, Ardabil, Iran
[b] Chemical Injuries Research Center, Systems Biology and Poisonings Institute, Baqiyatallah University of Medical Sciences, Tehran, Iran
[c] Faculty of Chemistry, Bu-Ali Sina University, Hamedan, Iran

ARTICLE INFO

Keywords:
Biosensors
Molecular imprinted polymers
VEGF and EGFR
Liposomal nanoparticles
Potentiometric striping analysis

ABSTRACT

This work demonstrates the development of a gold screen-printed electrode (Au-SPE)-based biosensor modified with a molecularly imprinted polymer and amplified using antibody-conjugated nano-liposomes. The developed biosensor was utilized for dual determination of epidermal growth factor receptor (EGFR) and vascular endothelial growth factor (VEGF) as cancer biomarkers. To prepare this biosensor, Au-SPE was modified with 3,3′-dithiodipropionic acid di(N-hydroxysuccinimide ester) via self-assembly method and then the target proteins (EGFR and VEGF) were covalently attached to the modified SPE. To synthesize the molecularly imprinted polymer, monomers of acrylamide and N,N′-methylenebis(acrylamide) were polymerized around the EGFR and VEGF templates, and to characterize the prepared biosensor, electrochemical impedance spectroscopy was used for analyses of surface changes in the engineered electrodes.

To produce reliable electrochemical signals, nano-liposomes which were loaded with Cd(II) and Cu(II) cations and decorated with antibodies specific for EGFR and VEGF were used as an efficient tool for detection of target biomarkers. In the analysis step, potentiometric striping analysis (PSA), as an electrochemical technique, was utilized for sensitive determination of these cations. The limits of detection (LODs) of EGFR and VEGF analyses were found to be 0.01 and 0.005 pg mL^{-1} with the linear dynamic ranges (LDRs) of 0.05–50000 and 0.01–7000 pg mL^{-1}, respectively. Moreover, the proposed biosensor was successfully used for sensitive, reproducible, and specific detection of EGFR and VEGF in real samples. Due to the SPE nature of the developed biosensor, we envision that this sensing tool has capability of being integrated with lab-on-a-chip (LOC), microfluidics, and micro total analysis systems.

1. Introduction

Miniaturized biosensors based on screen printed electrodes (SPE) for detection of multiple cancer biomarkers are an emerging tool for rapid, easy, and cost-effective detection of varieties of analytes (Arduini et al., 2016; Moreira et al., 2016; Patris et al., 2014). This type of sensors and biosensors often offer advantages over conventional methods. They allow researchers even non-specialist personnel to perform a large number of experiments with tiny volume of samples (Karami et al., 2017; Majidi et al., 2016). Since SPE can be successfully integrated with lab-on-a-chip (LOC), microfluidics, or micro total analysis systems, these are fascinating tools for analytical scientists (Punter-Villagrasa et al., 2014; Tüdős et al., 2001).

Cancer biomarkers are valuable in the early diagnosis, evaluation of chemotherapy, and demonstration of recurrence following chemotherapy (Afsharan et al., 2016; Johari-Ahar et al., 2015; Ludwig and Weinstein, 2005). For robust detection and evaluation process, physicians often request the screening of multiple markers to reach adequate sensitivity and selectivity of disease diagnosis. Technically, this multiple detection is a significant challenge for scientists in biosensor development; therefore, it is of great interest for varieties of analytical scientists.

Among cancer biomarkers, epidermal growth factor receptor (EGFR) and vascular endothelial growth factor (VEGF) have been recently proposed as valuable cancer biomarkers. Analysis of EGFR in the serum sample made possible early prediction of probability of response, progression-free survival (PFS), and overall survival (OS) in cancer patients (Gaafar et al., 2010; Hudelist et al., 2006), and VEGF is also a

* Corresponding author.
E-mail addresses: h.bagheri82@gmail.com, h.bagheri@bmsu.ac.ir (H. Bagheri).

https://doi.org/10.1016/j.bios.2018.02.005
Received 30 November 2017; Received in revised form 29 January 2018; Accepted 1 February 2018
Available online 03 February 2018
0956-5663/

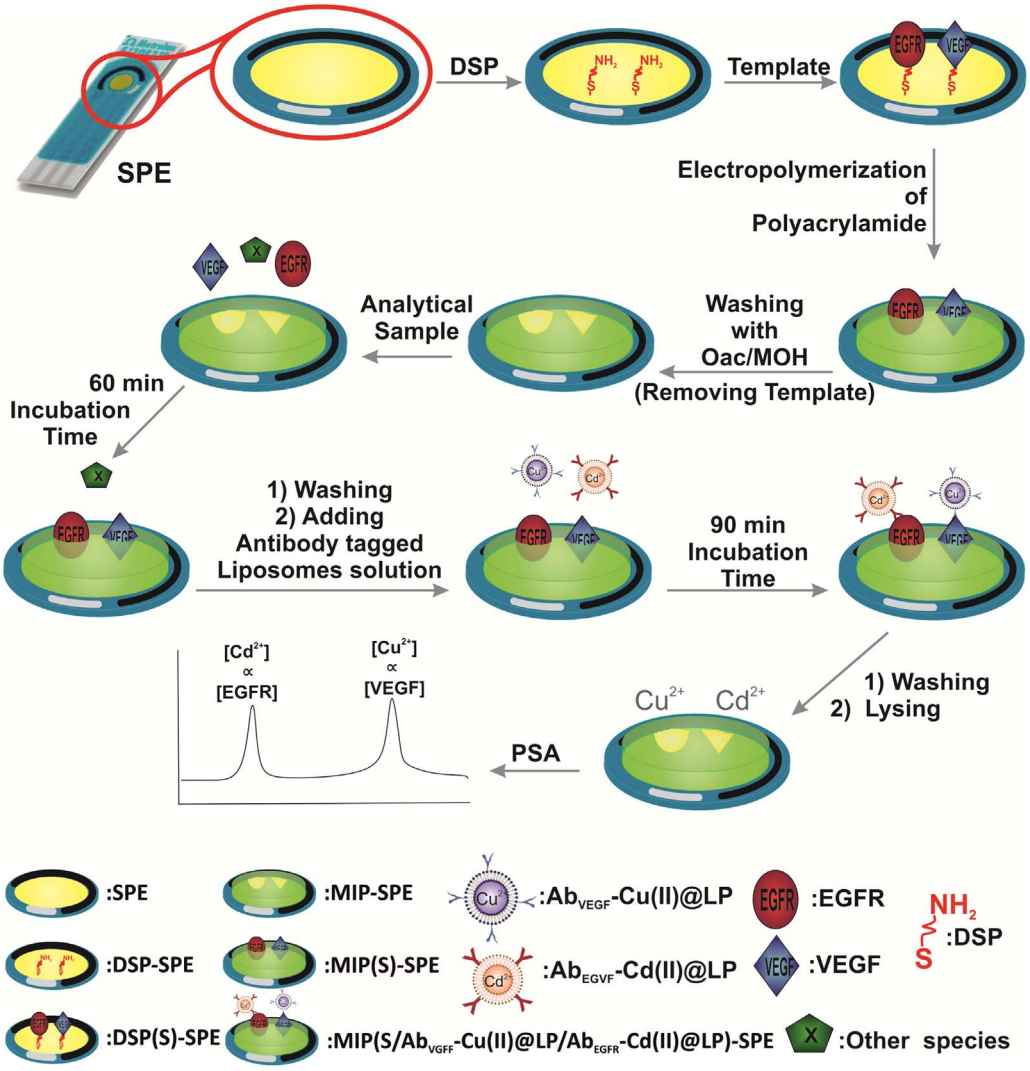

Scheme 1. Representation for the engineering processes of EGFR/VEGF biosensor.

signaling protein that is used in early diagnosis and metastasis detection of cancer (Herrlinger et al., 2004; Tamura et al., 2001; Zhou et al., 2009). However, concurrent detection of COX-2, EGFR, and VEGF-C have been proposed as an index for early diagnosis, recurrence prediction, and outcome evaluation for patients with endometrial carcinoma (Cai et al., 2017).

To date, various techniques have been reported for detection of EGFR and VEGF. For the detection of EGFR, quantum dot-based optical sensing (Ren et al., 2016; Wegner et al., 2014), surface plasmon resonance (Liu et al., 2011), scanning electrochemical microscopy (Takahashi et al., 2009), microfluidic biosensors (Regiart et al., 2017; Tian et al., 2017), impedimetric immunosensor (Elshafey et al., 2013b), nanoparticle-based detection (Mousavi et al., 2017; Vasudev et al., 2013), aptamer (Ilyas et al., 2012; Wan et al., 2012; Wang et al., 2012), peptide ligand (Li et al., 2013b), and aptamer-antibody based sandwich immunosensing (Ilkhani et al., 2015) have been proposed. For VEGF detection, electrochemical (Fu et al., 2016b), field effect transistor (Lee et al., 2009), optical (Freeman et al., 2012), capacitive (Qureshi et al., 2015) aptamer-based biosensors and molecular fluorescence endoscopy (Tjalma et al., 2016) have been proposed. However, there are few works reported for simultaneous detection of EGFR and VEGF. Until now, Kim et al. utilized fluorescence-Raman endoscopy in colorectal cancer imaging (Kim et al., 2017). In this study, we investigate the application of molecularly imprinted polymers (MIP) as the capture element and antibody-conjugated liposomes as a detection element for concurrent detection of VEGF and EGFR in serum samples. This work represents a novel strategy for simultaneous detection of biomarkers via efficient liposomal (LP) amplification strategy.

Molecularly imprinted polymers (MIPs) are emerging recognition elements that are selective to the analyte template, which can be considered as plastic antibody. In contrast to antibodies, MIPs have higher chemical and thermal stability, while being cost-effective and user-friendly (Canfarotta et al., 2016).

Recently, MIP-based electrochemical sensors/biosensor(s), which utilize MIP as recognition element, have been extensively used (Chen et al., 2011; Kryscio and Peppas, 2012; Song et al., 2014). However, there is no report on the development of electrochemical biosensors based on both MIP and antibodies for sandwich assay in dual detection of EGFR and VEGF.

2. Materials and methods

2.1. Chemicals

$K_4[Fe(CN)_6]$, $K_3[Fe(CN)_6]$, K_2HPO_4 and KH_2PO_4 were purchased from Merck Co., (Darmstadt, Germany). Acrylamide (AAM) and N, N′-methylenebisacrylamide (NNMBA), ammonium persulphate (APS), oxalic acid (OXA), and sodium chloride were from Fluka. Potassium chloride, sodium chloride, cadmium (II) nitrate and copper (II) sulfate pentahydrate were purchased from Sigma-Aldrich Chemical Co. (St.

Louis, MO). Dipalmitoylphosphatidylcholine (DPPC) and phosphatidylethanolamine (PE) were obtained from Avanti Polar Lipids (Alabaster, AL). Sulfo-SMCC (succinimidyl-4-(N-maleimidomethyl) cyclohexane-1-carboxylate) was purchased from Thermo Scientific™ Pierce™ (Waltham, Massachusetts, USA). Monoclonal anti-EGFR antibody and EGFR protein were procured from Abnova. Phosphate buffered saline (PBS, 10 mM with pH 7.4) was prepared by dissolving 1 tablet in 200 µL of deionized (DI) water and used to prepare the Anti-EGFR antibody (1 mg mL^{-1}) and EGFR solutions. Recombinant human VEGF165 was purchased from R&D systems (Minneapolis, USA) and reconstituted in ultrapure water prior to use. Anti-human VEGF Ab was purchased from Abcam (Toronto, Canada). All solutions were prepared with deionized water having a resistivity not less than 18 MΩ cm (Milli-Q, Bedford, MA). 3,3′-dithiodipropionic acid di(N-hydroxysuccinimide ester) (DSP) was purchased from Sigma -Aldrich (Milwaukee, USA). Human VEGF and EGFR ELISA Kit were prepared from Thermo Fisher Scientific (Waltham, Massachusetts, US).

2.2. Fabrication of biosensor

2.2.1. Self-assembly and characterization of monolayer of DSP on SPE

All fabrication steps of the engineered biosensor are schematically illustrated in Scheme 1. Self-assembled monolayers (SAMs) of thiols on SPE (DSP-SPE) were prepared by immersing clean electrodes in the 10 mM aqueous solution of DSP under shaking (50 rpm) at room temperature and dark for 60 h. During this period, SAMs were studied using ESI, and R_{ct} values were plotted as a function of time. The prepared DSP-SPE was washed with ultrapure water and then dried under nitrogen stream.

2.2.2. Architecture of MIP on DSP-SPE

DSP-SPE was incubated with EGFR and VEGF protein (ratio: 1:1) for 24 h to form a covalent bond on the electrode surface via amide bond formation. Then, unreacted sites on the DSP-SPE were blocked with AAM monomer by immersing DSP-SPE in an AAM monomer solution (10% w v^{-1}) for 24 h. In the next step, to form MIP on the SPE (MIP(s)-SPE), AAM and NNMBA were polymerized using persulphate (Moreira et al., 2013). This imprinting stage was started by deposition of 25 µL of AAM (10 mM) and 25 µL of NNMBA (70 mM) solution on DSP-SPE. This was followed by the addition of 10 µL of APS solution (60 mM) in PBS (pH 7.4). The polymerization process at different time points was stopped by the addition of hydroquinone solution in ethanol (w/t, 1%). Finally, the template molecules which were trapped in MIP were removed from MIP(s)-SPE incubated in the dilute solution of OXA for 12 h. OXA is able to break peptide bonds, allowing a successful removal of the template molecules from the imprinted layer (Bonini et al., 2007). The imprinted sensor was washed with PBS solution. All steps were monitored using EIS.

2.2.3. Preparation of $Cd(NO_3)_2$ or $CuSO_4$-loaded LPs

Cu(II) and Cd(II)-loaded liposomes (Cu(II)@LP and Cd(II)@LP) were prepared by thin film layer hydration method based on the previously reported method (Han et al., 2017) with some minor modification. Briefly, 1, 2-dipalmitoyl-*sn*-glycero-3-phosphocholine (DPPC, 850335, Avanti Lipids, Alabaster, AL, phase-transition temperature of 41 °C), cholesterol, and PE with a mass ratio of 3:1:1 were dissolved in chloroform/methanol (9:1, v/v). Organic solvents were evaporated to make a thin film in a glass bottle. Then, the bottle was settled in vacuum overnight to completely remove the organic solvents. The thin film was hydrated with phosphate-buffered saline (PBS, pH 7.4) containing $Cd(NO_3)_2$ or $CuSO_4$ (150 mM) at 50 °C in a sonication bath for 30 min to obtain multi-lamellar liposomes. Afterwards, the liposomes were homogenized using ultra-sonication for 10 min (VC750, Sonics & Materials, and Newton, CT) to produce nanosized liposomes. All preparations were performed under nitrogen. To remove the un-encapsulated Cd $(NO_3)_2$ or $CuSO_4$, the solution was centrifuged at 1000 rpm for 15 min and the supernatant remained. Then, Cu(II)@LP and Cd(II)@LP were harvested by centrifugation of the supernatant at 8000 rpm for 15 min. The final Cu(II)@LP and Cd(II)@LP were washed with PBS and stored at 4 °C.

2.2.4. Conjugation of Ab_{EGFR} and Ab_{VEGF} with Cd(II)@LP and Cu(II)@LP, respectively

Amine groups on PE molecules that were incorporated in the structure in the synthesis of LP NPs were activated using hetero-bifunctional crosslinking agent (i.e., sulfo-SMCC). Then, EGFR and VEGF antibodies are conjugated onto the surface of liposomes via sulfhydryl residues that react with sulfo-SMCC (Hashida and Ishikawa, 1985; Dewey et al., 1987). For the preparation of mAb-conjugated LPs, 5 mg of Cd(II)@LP and Cu(II)@LP were dissolved in 1 mL of PBS buffer (0.1 M, pH 7.4). Then, 2 mg of sulfo-SMCC was added to the prepared solutions-molar ratio of sulfo-SMCC to LPs was 80:1– and after 1 h, maleimide-activated LPs were filtered through an Amicon ultra-0.5 mL centrifugal filter (EMD Millipore Amicon™, MW cut-off 3 kDa) via centrifugation at 12,000*g* using a Sigma 1–15P refrigerated centrifuge (Sartorius Stedim Biotech, GmbH, Germany) for 10 min. Subsequently, maleimide-activated LPs were mixed at the desired molar ratio (7:1, µgm Ab/µg LPs) with a mAb dissolved in PBS (0.1 M, pH: 7.4). The reaction mixtures were incubated overnight (at 4 °C on a shaker). Finally, the reaction mixture was passed through a Sephadex G-75 column to separate the mAb-tagged LPs from free mAb. These LP suspensions were freeze-dried and stored at 4 °C until required for use.

2.3. Assessment of biosensor performance

For performance assessment of the engineered biosensor, MIP-SPE was exposed to the standard solutions of VEGF and EGFR proteins, and then washed with buffer solution (Scheme 1) to form MIP(S)-SPE. Next, MIP(S)-SPE were incubated with Ab_{EGFR}-Cd(II)@LP and Ab_{VEGF}-Cu(II)@LP for 90 min, and after being washed with a very dilute solution of triton X100, PSA analyses were carried out to measure electrochemical signals. Prior to PSA analyses, lysing buffer was used to crack Ab_{EGFR}-Cd(II)@LP, Ab_{VEGF}-Cu(II)@LP LPs and template molecules attached to MIP(S)-SPE. The concentrations of Cd(II) and Cu(II), which were measured using PSA, were indirectly indicative of EGFR and VEGF concentrations. The condition in which PSA measurements were performed included applying − 1.2 V as conditional potential (E_{ac}) for 240 s in the pre-treatment step (t_{ac}) and then applying constant current (i_s) of + 5 µA and recording electrochemical signals ranging from −1 to 0.0 V. Moreover, the calibration curve was plotted by addition of known concentrations of VEGF and EGFR in the real samples. To prepare serum samples for real sample analyses, whole blood samples were collected in untreated BD Vacutainer Serum tubes (Cat #: 367812) and then incubated undisturbed at room temperature for 20 min. The samples were centrifuged at 3000 rpm for 10 min at 4 °C and the supernatants (serum samples) were immediately aliquoted and frozen at − 80 °C.

2.4. Electrochemical impedance spectroscopy (EIS) and particle size analyses

All electrochemical measurements other than EIS analyses were performed using an Autolab PGSTAT30 Potentiostat/Galvanostat equipped with GPES 4.7 software (Eco-Chemie, Utrecht, Netherland). The EIS measurements were also carried out using an Autolab PGSTAT302N (Metrohm Co., Schiedam, Netherlands) equipped with a frequency response analyzer (FRA) module and Nova 1.8 software. Commercial screen-printed electrodes (Metrohm Co., Schiedam, Netherland, code: 6.1208.210) were composed of a working electrode (gold, diameter of 4 mm), carbon-based counter electrode and silver pseudo-reference electrode. The connection of SPE to the Autolab is provided by a specific homemade connector. All laboratory

experiments were conducted at ambient condition (25 °C), and measurements on SPE were performed by placing a drop (50 μL) of the corresponding solution on the working area. All EIS experiments, which were performed within a frequency range of 0.1 Hz to 100 kHz at the formal potential of redox couple $Fe(CN)_6^{4-/3-}$ (0.17 V), were recorded in the solution containing 5 mM $K_3[Fe(CN)_6]/K_4[Fe(CN)_6]$ (1:1) and PBS (0.1 M, pH 7). The impedance data were represented in the form of a complex plot (Nyquist plot), and the fitting program of AUTO-LAB (Nova 1.8) was used to analyze the impedance spectra with an appropriate equivalent electrical circuit.

To determine the dynamic diameter and zeta potential of the engineered LPs, we performed dynamic light scattering (DLS) analyses using Nanotrac Wave™ (Microtrac, San Diego, CA, USA). The size of LPs was calculated by fitting the data to a polydispersed model using the Dynamics software version 5.26 (Microtrac, San Diego, CA, USA).

3. Results and discussion

3.1. Characterization

3.1.1. EIS analyses

EIS is one of the most powerful techniques that are used in the field of interfacial chemistry to study the successful immobilization of molecules (i.e., MIP or nanoparticles) onto the electrode surface. Fig. 1 (panel A) represents the EIS-derived interfacial electron transfer phenomena of bare SPE (curve a), DSP-SPE (curve b), DSP(S)-SPE (curve c), MIP-SPE (curve d), MIP(S)-SPE (curve e), MIP(S/Ab_{VEGF}-Cu(II)@LP)-SPE (curve f), MIP(S/Ab_{EGFR}-Cd(II)@LP)-SPE (curve g), and MIP(S/Ab_{EGFR}-Cd(II)@LP/Ab_{VEGF}-Cu(II)@LP)-SPE (curve h). In the Nyquist plot, the diameter of semicircles represents a faradaic resistance that reflects charge transfer resistance (R_{ct}) of the electrodes. Moreover, Warburg impedance is observed at low frequencies. In the first step towards developing the engineered biosensor, self-assembly of DSP on the bare SPE significantly increased the R_{ct} value, representing the nonconductive nature of DSP (curve b). Following the immobilization of EGFR and VEGF molecules on the DSP-SPE (DSP(S)-SPE), the R_{ct} value was slightly increased (curve c), which was due to the increased resistance of the double layer. Formation of MIP on the DSP(S)-SPE (MIP(S)-SPE) clearly increased the R_{ct} value (curve e). However, after MIP(S)-SPE was incubated with OXA solution, it was observed that the R_{ct} value of MIP-SPE was considerably decreased (curve d). It seems that removal of templates from the electrode surface permits electrons to be transferred through the formed holes at the electrode, resulting in enhancement of the charge transfer rate.

Incubation of MIP-SPE with EGFR and VEGF significantly increased R_{ct}, indicating a specific interaction of these proteins with holes in MIP. In the next step, incubation of MIP(S)-SPE with Ab_{VEGF}-Cu(II)@LP (curve f) and Ab_{EGFR}-Cd(II)@LP (curve g), or with both of them (curve h) increased the R_{ct} values, showing that the lipid-based nature of LPs can impede the charges to be transferred through the electrode layers (Alfonta et al., 2001; Damhorst et al., 2013).

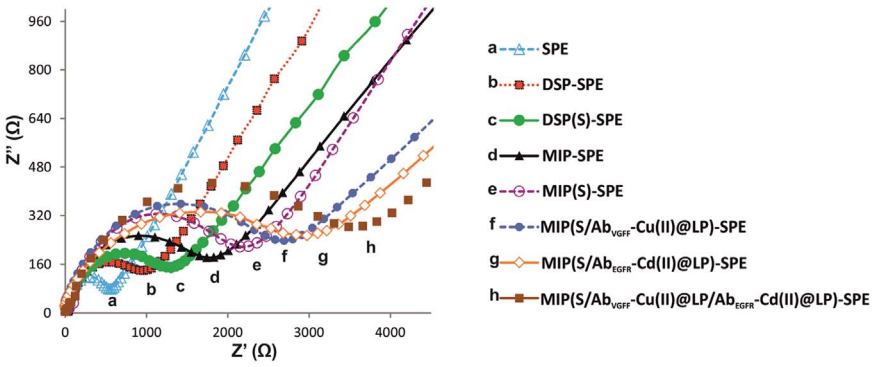

Fig. 1. Electrochemical impedance spectroscopy (EIS) of step-by-step modification of the engineered biosensor. Bare SPE (curve a), DSP-SPE (curve b), DSP(S)-SPE (curve c), MIP-SPE (curve d), MIP (S)-SPE (curve e), MIP(S/Ab_{VEGF}-Cu(II)@LP)-SPE (curve d), MIP (S/Ab_{EGFR}-Cd(II)@LP)-SPE (curve e), and MIP(S/Ab_{EGFR}-Cd(II)@LP/Ab_{VEGF}-Cu(II)@LP)-SPE (curve f). EIS measurements were performed in 5 mM $K_3[Fe(CN)_6]/K_4[Fe(CN)_6]$ in phosphate buffer, pH 7, using a bios voltage of 0.17 V and the frequency range of 0.1 Hz to 100 kHz.

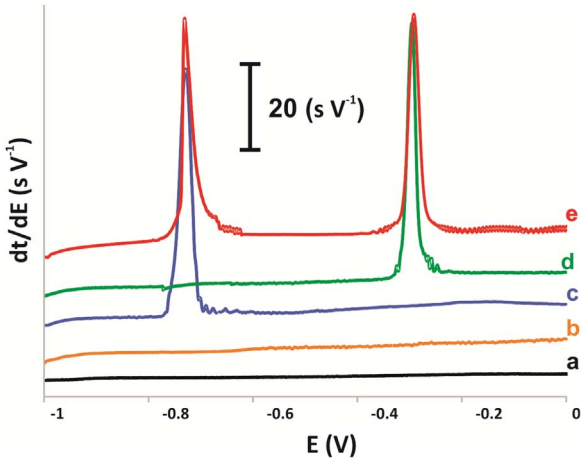

Fig. 2. Potentiometric stripping analysis (PSA) of the bare SPE (curve a) and MIP-SPE before (curve b) and after incubation with 770 pg mL^{-1} EGFR (curve c), 100 pg mL^{-1} VEGF (curve d), and both of them (curve e).

3.1.2. Analyses of samples using PSA

PSA is one the powerful techniques that can sensitively analyze most cations even in the presence of interfering species in real samples (Jagner, 1982; La Pera et al., 2002; Tarley et al., 2009). In this regard, we selected PSA as the preferred technique for sample analyses. Fig. 2 represents PSA results of the bare SPE (curve a) and MIP(S)-SPE before (curve b) and after incubation with 700 pg mL^{-1} EGFR (curve c), 100 pg mL^{-1} VEGF (curve d) and both of them (curve e). It should be stated that PSA signals were recorded after lysing buffer addition. In the absence of analytes (VEGF or EGFR) bare SPE (curve a) and MIP-SPE (curve b) showed no signals in the presence of methanol and OXA. Then, MIP-SPE was incubated with EGFR and next with corresponding liposome. After the lysis of liposomes specifically attached to MIP-SPE, cadmium ions were released into the solution and produced a peak at − 0.73 V. The height of the peak was proportional to the concentration of EGFR (curve c). Similarly, MIP-SPE was incubated with VEGF and corresponding liposome, and using PSA analysis, the released Cu(II) ions represented a signal at − 0.3 V. The peak height was related to the VEGF concentration (curve d). For the simultaneous detection of EGFR and VEGF, MIP-SPE was introduced into the mixture of VEGF and EGFR, and after the lysing step, the released Cd(II) and Cu(II) generated their distinguished signals in the PSA analyses, with which the intensity of the produced signals and EGFR/VEGF concentration were in close correspondence (curve e).

3.1.3. Dynamic light scattering (DLS) analyses

As shown in Fig. 3, assessment of the size distribution revealed that the mean diameters of Cd(II)@LP (Panel A), Cu(II)@LP (Panel C), Ab_{EGFR}-Cd(II)@LP (Panel B), and Ab_{VEGF}-Cu(II)@LP (Panel D) were 61, 54, 84, and 76 nm, respectively. These results show that the size

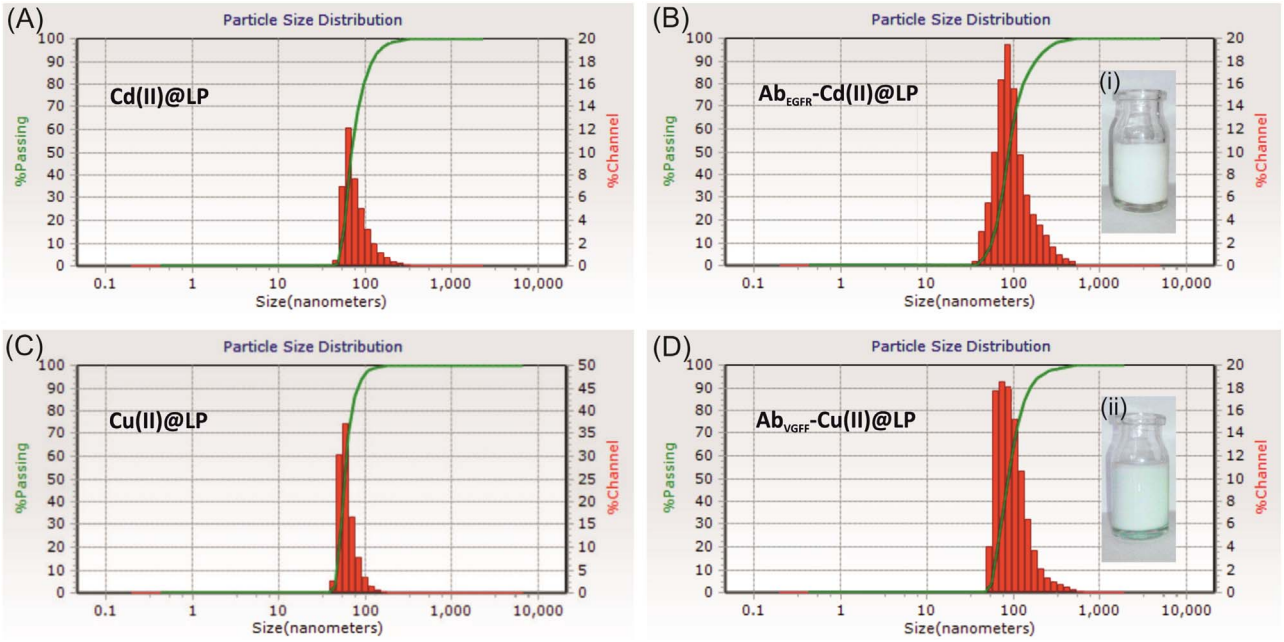

Fig. 3. Dynamic light scattering (DLS) analyses of (A) Cd(II)@LP, (B) Ab_{EGFR}-Cd(II)@LP, (C) Cu(II)@LP, and (D) Ab_{VEGF}-Cu(II)@LP. Inset: Images of the prepared Ab_{EGFR}-Cd(II)@LP (inset i), and Ab_{VEGF}-Cu(II)@LP (inset ii).

distributions of Cd(II)@LP and Cu(II)@LP are in the same range, and by modifying LPs using mAb, the mean diameters slightly increase. In addition, Fig. 3 inset panels B (i) and D (ii) represent the prepared Ab_{EGFR}-Cd(II)@LP and Ab_{VEGF}-Cu(II)@LP nanoparticles, respectively. A number of studies have reported utilization of DLS for characterization of Ab-conjugated nano-LPs. Song et al. reported the development of anti-HIF-1α antibody-conjugated unimolecular polymer nano micelles filled with Paclitaxel (PTX) for cancer targeting therapy (Song et al., 2010). They characterized the resultant anti-HIF-1α conjugated nano micelles filled with PTX (anti-HIF-1α-NMs-PTX nanocomposites) using DLS and showed that with conjugation of anti-HIF-1α to nano micelles, their dynamic diameter was increased. In another study, Gao et al. prepared nano LPs conjugated with anti-EGFR Ab for small interfering RNA (siRNA) delivery and observed the size of naked and conjugated liposomes by DLS (Gao et al., 2011). Kim et al. prepared pH-sensitive, long-circulating and EGFR-targeted immunoliposomes and measured physicochemical properties of the prepared immunoliposomes by SEM and DLS (Kim et al., 2008). However, our results were in close agreement with that of obtained from previous studies.

3.2. Optimization of the experimental parameters

3.2.1. Self-assembly of DSP on a gold electrode

Self-assembly of organic linkers containing functional groups can provide stable and uniform anchors on the electrode surface for designing biosensor architectures (Frasconi et al., 2010; Phares et al., 2009). As can be seen in the structure of DSP, the sulfhydryl group offers an invaluable tool for the attachment of biosensor elements to gold surfaces. In addition, DSP has reactive ester groups that make connections with amine or thiol-containing agents.

To construct the first layer of the biosensor, we allowed DSP to be self-assembled on SPE and checked the pack density of DSP using the EIS technique to monitor the completion of assembling. Fig. S1, panel A (See Supplementary material) shows the results of Rct analyses for self-assembly of DSP on the bare SPE monitored using EIS at different incubation time points. The results revealed that after 60 h of incubation time, self-assembly of DSP became complete and R_{ct} showed no changes. More assessments with fitness analysis demonstrated that the SPE surface was decorated uniformly with DSP. As a result, it seems that DSP is a good candidate for the construction of the biosensor foundation. There is only a study that (Yuan et al., 2015) introduced DSP to gold nanoparticles and then used these modified nanoparticles for colorimetric detection of hydrogen sulfide.

3.2.2. Engineering the thickness of polymerized MIP

The study on the thickness of polymerized MIP shows that it has a critical effect on the successful and specific detection of the analytes. Fig. S1, panel B (See Supplementary material) represents the results of R_{ct} analyses of MIP polymerization on DSP(S)-SPE before (a) and after (b) incubation with OXA solution. During the polymerization process, at a series of different time points, stop solution was added to DSP(S)-SPE to quench MIP polymerization, allowing the formation of MIP with a different width. As predicted, with an increase in MIP thickness, R_{ct} also increased and reached its maximum value. The EIS results from incubation of the prepared MIP(S)-SPE with a different width in the solution of OXA in methanol clearly demonstrated that 30 min is the optimum time for preparation of MIP. It seems that at this thickness, analyte molecules face the lysing solution, and a greater increase in thickness can cover the analyte surface and significantly increase R_{ct}. It is evident that providing additional time for MIP polymerization stops the lysis of analytes and disturbs the charge transfer through electrode layers.

3.2.3. Lysing condition of mAb conjugated Cd(II)@LP and Cu(II)@LP

To study lysing LPs, mixtures of OXA (20%) and pure methanol (MOH) with various ratios (V/V, 4:1, 3:1, 2:1, 1:1, 1:2, 1:1, 1:3, 1:4) were investigated (Fig. S1, panel C, See Supplementary material). In each lysing experiment, 100 µL of mAb-conjugated Cd(II)@LP and Cu (II)@LP was transferred to a micro tube, and then, 200 µL of lysing agent was added to the LP solutions. Then, the mixture was mixed using a vortex for 3 min. Subsequently, 100 µL of the mixture was mounted on the MIP-SPE, and the release of Cu(II) and Cd(II) was demonstrated using PSA. The maximum response was recorded with the ratio of 3:1 (V/V).

3.2.4. Temperature and time optimization for interaction of templates with MIP-SPE

Using the EIS technique, the formation of complex between the

analyte (template: EGFR and VEGF) and MIP-SPE was studied at five temperatures. As can be seen in Fig. S2, panel A (See Supplementary material) with an increase in temperature from 4 °C to 35 °C, Rct increased until it reached its maximum value, representing that the maximum sites on MIP were occupied with analyte molecules, while higher temperatures led to the significant decrease in Rct, suggesting that folding changes may alter the interaction of the analyte and MIP. However, the optimum temperature for the interaction of analytes with MIP-SPE was found to be 35 °C.

To find the optimum duration for completion of complex formation between analytes and MIP-SPE, Rct values were recorded at different time points using EIS. These results, as shown in Fig. S2, panel B (See Supplementary material) indicate that EGFR more rapidly than VEGF binds to MIP. In addition, the optimum time needed for analytes and the MIP-SPE complex was found to be 60 min.

3.2.5. Optimization of the incubation temperature and incubation time for liposomes

To determine the optimum temperature for incubation of Ab_{EGFR}-Cd(II)@LP and Ab_{VEGF}-Cu(II)@LP with MIP(S)-SPE, R_{ct} values that were recorded from EIS analyses of MIP(S)-SPE were plotted at five temperatures. The results, which are shown in Fig. S2, panel C (See Supplementary material), clearly indicate that 35 °C is an optimum point of incubation. However, at temperatures higher than 35 °C, the R_{ct} value is identical to that of MIP(S)-SPE, suggesting that no analyte molecules can attach to the electrode surface and proposing the idea that mAb molecules on the Ab_{EGFR}-Cd(II)@LP, and Ab_{VEGF}-Cu(II)@LP perhaps have lost their folding.

To find the optimum time for successful incubation of Ab_{EGFR}-Cd(II)@LP, and Ab_{VEGF}-Cu(II)@LP with MIP(S)-SPE, R_{ct} values were measured using EIS at different time points. From these values, as shown in Fig. S2, panel D (See Supplementary material), it can be realized that in contrast to each other, VEGF can form a complex with MIP(S)-SPE more rapidly than EGFR. However, the optimum time that is suitable for both interactions was found to be 90 min. At times greater than 90 min, no changes in R_{ct} can be observed, indicating that almost all sites on MIP (S)-SPE were occupied, while allocation of extra time did not improve the complex process.

3.2.6. Optimization of the PSA parameters

The stripping current (i_s), accumulation potential (E_{ac}) and accumulation (t_{ac}) in PSA experiments were optimized in our study using MIP-SPE. E_{ac} was optimized by keeping i_s at + 10 μA and t_{ac} at 100 s. With these values, E_{ac} was determined by applying a potential window of − 0.3 to − 1.4 V. As shown in Fig. S3 (panel A, See Supplementary material), the PSA signals of 100 μM of Cu (II) (curve a) and Cd(II) (curve b) reached its maximum value at − 1.0 and − 1.2 V respectively. Therefore, the E_{ac} value of − 1.2 V was considered for further studies.

Further, the determination of optimal t_{ac} is also one of the crucial parameters that may improve the sensitivity of detection in PSA experiments. The effect of applied t_{ac} on the intensity of PSA signals was studied over a period of 60–300 s (Fig. S3, panel B, See Supplementary material) by keeping i_s at + 10 μA and E_{ac} at − 1.2 V. It was found that there was an increase in the PSA signal of Cu(II) and Cd(II) up to 240 (curve a) and 210 s (curve b) respectively, whereas the PSA signal became stable after 240 s. Thus, the maximum PSA signal was obtained at the t_{ac} value of 240 s, which was selected as an optimal time for the detection of Cu(II) and Cd(II) with the highest sensitivity.

Finally, keeping E_{ac} at − 1.2 V and t_{ac} at 240 s, i_s was studied ranging from 1 to 70 μA. During the stripping step, the rate of chemical oxidation per-concentrated Cu to Cu(II) and Cd to Cd(II) at normal conditions without applying potential or current on the working electrode is very slow. Thus, constant current needs to be applied for fast electrochemical determination. In fact, without applying external current to the working electrode, a long period of time is needed for Cu and Cd to be oxidized, while the oxidation of Cu and Cd appears to be accelerated by applying i_s. In this study, it was also observed that when the applied i_s was decreased from 70 μA to 1 μA, the rate of oxidation of Cu and Cd decreased and PSA signals increased significantly (Fig. S3, panel C, See Supplementary material). It seems that not only does the PSA signal increase by the lowered i_s, but also the background PSA signals can concurrently increase, which are considered as detection noises. Therefore, a middle value (approximately + 5 μA) was considered as an optimal stripping current. Therefore, the final conditions for an optimal PSA were found to be E_{ac} = − 1.2 V, t_{ac} = 240 s and i_s = + 5 μA.

3.3. Analytical application

3.3.1. Calibration curve and LOD

Fig. S4 (See Supplementary material) presents the PSA signals of different concentrations of VEGF (panel A and B) and EGFR (panel C and D). The recorded signals were found to be linear in the ranges (LDR) of 0.05–50000 and 0.01–7000 pg $mL^{-1}$with a limit of detection (LOD) of 0.01 and 0.005 pg mL^{-1} for EGFR and VEGF, respectively. The cross-effect of EGFR and VEGF on the calibration curves was studied, and it was observed that the slope of the calibration curves showed no significant differences (Fig. 4, panel A, B and C).

In contrast to reported EGFR and VEGF sensors/biosensors, summarized in Table 1, our immunosensor does not need pre-preparation steps to reduce interference of electro-active species. In addition, because of the nature of the applied technique (PSA) and the structure of the recognition element (Ab), we envision that the engineered immunosensor has a number of superiorities in terms of sensitivity, selectivity, reproducibility, and LOD over the reported EGFR and VEGF biosensors.

3.3.2. Interference study

For the assessment of biosensor specificity, multiple biomarkers including cortisol (COR), neuron specific enolase (NSE), prostate-specific antigen (PSA), human thrombin (HTR), human immunoglobulin (IgG), human albumin serum (HAS), bovine serum albumin (BSA), thrombin antigen (TA) and carcinoembryonic antigen (CEA) were tested and the charge transfer rate was monitored using EIS. The results in Fig. 4 (panel D) show the EIS analysis of the engineered biosensor in the presence of these counterparts. The Ret values for the interfering species were significantly ($p < 0.05$) lower than those of EGFR and VEGF and were similar to the values of blank samples (R_{et} = 992.97 ± 2.59). These data clearly imply that the immunosensor can specifically sense the target oncomarker, EGFR and VEGF.

3.3.3. Real sample analysis

The potential application of the developed biosensor was investigated by measuring the EGFR and VEFG concentration in serum samples. The engineered biosensor showed great detection potential in comparison with ELISA (Table S1, See Supplementary material). We found that there is no significant difference between the results obtained from the engineered PSA-based biosensor and the ELISA method ($p < 0.05$). Further, it should be highlighted that the presence of proteins other than VEGF and EGFR in the serum showed no remarkable effect(s) on the sensitivity and specificity of the engineered PSA-based biosensor.

3.3.4. Reproducibility and stability of the biosensor

To evaluate the reproducibility of the prepared biosensors, a series of the independently prepared electrodes were used for analyses of one sample at the fixed concentration of EGFR and VEGF. Coefficient variation (CV) of the measurements was found to be 3.2%, reflecting the reproducibility of the proposed biosensor was quite good.

Technically, the developed biosensor is comprised of three main parts including MIP(S)-SPE, Ab_{EGFR}-Cd(II)@LP, and Ab_{VEGF}-Cu(II)@LP.

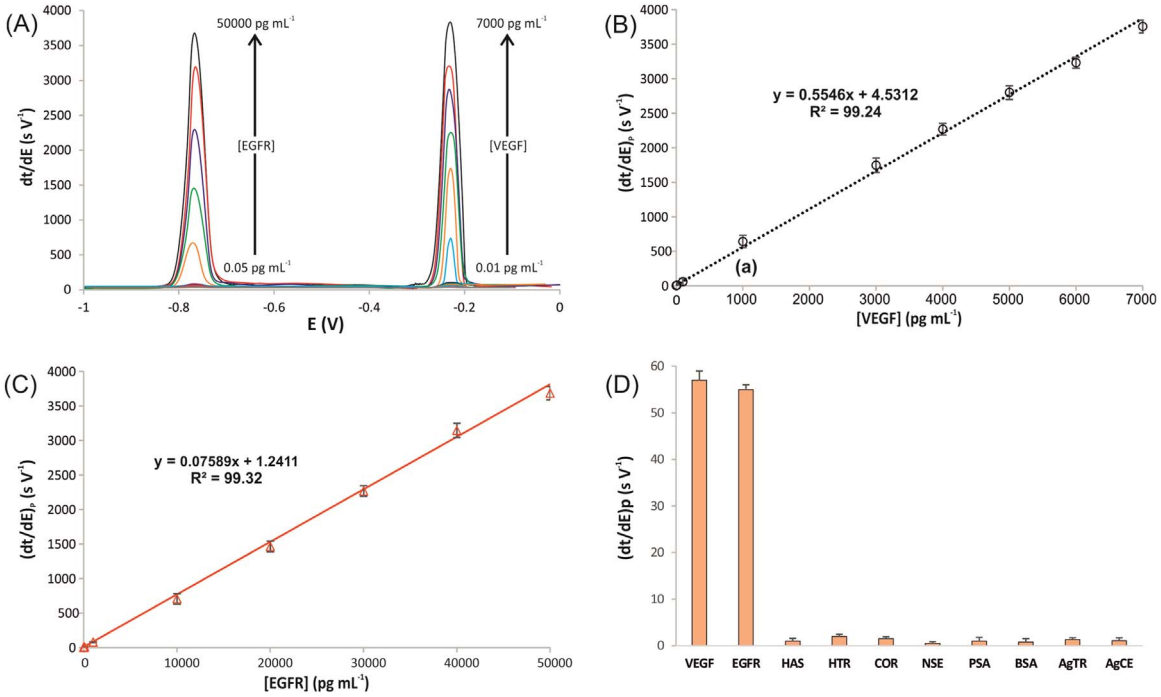

Fig. 4. Potentiometric stripping analyses (PSA) and interference study of the developed biosensor. (A) PSA of VEGF (0.01–7000 pg mL^{-1}) in the presence of EGFR (0.05–50000 pg mL^{-1}) with different concentrations. (B) Calibration curve of the VEGF analyses in the presence of EGFR. (C) Calibration curve of the EGFR analyses in the presence of VEGF. (D) Interference study of the developed biosensor: PSA of VEGF (100 pg mL^{-1}) and EGFR (700 pg mL^{-1}) in the presence of 5000 pg mL^{-1} of COR, NSE, PSA, HTR, IgG, HAS, BSA, TRA, and CEA.

The stability of the prepared MIP-SPEs that were kept in deoxygenated PBS solution (10 mM, pH 7.4) containing sodium azide (0.02% w/v) and the stability of above-mentioned reagents were investigated during 60 days post-fabrication and 75 days post-preparation, respectively. CV of measurements (4.8%) showed that the stored electrodes were stable during 30 days post-fabrication, while Ab_{EGFR}-Cd(II)@LP, and Ab_{VEGF}-Cu(II)@LP were stable up to 60 days post-preparation—CV of measurements was less than 7%.

4. Conclusion

In recent years, with emergence of novel and potential biomarkers utilized in robust detection of diseases, multi-analyte sensing systems have been of great interest for biosensor engineers, but the development of such powerful tools that are able to simultaneously sense multiple markers is still challenging.

Technically, to develop novel and dual-analyte biosensor, we capitalized on the molecularly imprinted polymers (MIPs) and antibodies conjugated to liposomes which were loaded with electroactive agents. However, the engineered biosensor could specifically and sensitively sense EGFR and VEGF analytes and efficiently amplify the electrochemical signals from PSA measurements. This detecting system offered an improved LOD (0.01 pg mL^{-1} for EGFR and 0.005 pg mL^{-1} for VEGF) and broad LRD (0.05–50000 pg mL^{-1} for EGFR and

Table 1
Comparison of the proposed method with previously published electrochemical methods used for detection of EGFR and VEGF.

WE	Modifier	EGFR		VEGF		Technic	Ref.
		LDR (pg mL^{-1})	LOD (pg mL^{-1})	LDR (nM)	LOD (pM)		
AuE	CMK3-p(AC-*co*-MDHLA)-Ab_{EGFR}-AMS	10–50,000	3.03			A	(Regiart et al., 2017)
SPE	AuNPs-PG-Ab_{EGFR}	1–1,000,000	0.34			EIS	(Elshafey et al., 2013a)
SPE	DTSB-Ab_{EGFR}-EA	1–100,000	1			CV	(Vasudev et al., 2013)
SPE	PPL-FC	0. 1–1000	0.037			DPV	(Li et al., 2013a)
GCE	$Ab1_{EGFR}$-EGFR-$Ab2_{EGFR}$-PbNC@BSA	400–35,000	8			SWASV	(Mousavi et al., 2017)
GSPE	PT-Ab_{EGFR}-EGFR Fe_3O_4/TMC/Au	0–1000	0.05			DPV	(Omidfar et al., 2015)
SPE	rGO-P(AMAM)-Th-AuNC-Apt_{VEGF}			0.0025–0.320	0.7	DPV	(Tabrizi et al., 2017)
SPE	Apt_{VEGF}-MB			0.05–0.15	5	ACV	(Zhao et al., 2011)
AuWE	$Apt1_{VEGF}$-VEGF-$Apt2_{VEGF}$-PQQGDH			15–60	0.015	A	(Nonaka and Ikebukuro, 2012)
GCE	DNA-Ag/Pt NCs			0.006–0.02	4.6	A	(Fu et al., 2016a)
GSPE	AuNPs-$Apt1_{VEGF}$-VEGF-$Apt2_{VEGF}$-STV-AP			0–250	0.03	DPV	(Ravalli et al., 2015)
SPE	$Apt1_{VEGF}$-VEGF-$Apt2_{VEGF}$-Hem			0–80	0.001	DPV	(Lv et al., 2014)
SPE	MIP-Ab_{EGFR}-Cd(II)@LP-Ab_{VEGF}-Cu(II)@LP	0.05–50,000	0.01	0.01–7000 (pg mL^{-1})	0.005 (pg mL^{-1})	CC-PSA	This work

A: Amperometry, Ab: Antibody, ACV: Alternating current voltammetry, AMS: amino-functionalized mesoporous silica, AptVEGF: VEGF Aptamer, AuE: Gold electrode, AuNC: Gold nanocomposite, AuWE: Gold wire electrode, CMK3: Ordered mesoporous carbon, DNA-Ag/Pt NCs: DNA-templated Ag/Pt bimetallic nanoclusters, DTSP: Dithiobissuccinimidyl propionate, EA: Ethylenamine, Fc: ferrocene, Fe_3O_4/TMC/Au: Fe_3O_4/N trimethyl chitosan/gold nanocomposite, GCE: Glassy carbon electrode, GSPE: graphite screen printed electrode, Hem: Hemin, LDR: Linear dynamic range, LOD: Limit of detection, MB: Methylene blue, p(AC-*co*-MDHLA): poly(acrylamide-*co*-methacrylate of dihydrolipoic acid), p(AMAM) poly(amidoamine), PbNC@BSA: bovine serum albumin-templated Pb nanocluster, PG: Protein G, PPL: Peptide ligand, PQQGDH: pyrroquinoline quinone glucose dehydrogenase, PT: Polythiophene, Ref.: Reference, rGO: Reduced graphene oxide, SWASV: square wave anodic stripping voltammetric, STV-AP: streptavidin-alkaline phosphatase, Th: thionine, WE: Working electrode.

0.01–7000 pg mL^{-1} for VEGF) without any pre-separation step.

We envision that the engineered SPE-based biosensor is capable of being successfully integrated with lab-on-a-chip (LOC), microfluidics, or micro total analysis systems. In clinic, usually for final decision, an array of biomarkers are requested to be analyzed, and it seems that in the near future, more electrochemical biosensors are expected to be developed for multiplex sensing of biomarkers.

Acknowledgement

This research was supported by the Research Council of Baqiyatallah University of Medical Sciences. Also, the authors gratefully acknowledge the financial and instrumental supports provided by School of Pharmacy, Ardabil University of Medical Sciences, Ardabil, Iran.

Appendix A. Supplementary material

Supplementary data associated with this article can be found in the online version at http://dx.doi.org/10.1016/j.bios.2018.02.005.

References

Afsharan, H., Navaeipour, F., Khalilzadeh, B., Tajalli, H., Mollabashi, M., Ahar, M.J., Rashidi, M.-R., 2016. Biosens. Bioelectron. 80 (Suppl. C), S146–S153.
Alfonta, L., Singh, A.K., Willner, I., 2001. Anal. Chem. 73 (1), 91–102.
Arduini, F., Micheli, L., Moscone, D., Palleschi, G., Piermarini, S., Ricci, F., Volpe, G., 2016. TrAC Trends Anal. Chem. 79 (Suppl. C), S114–S126.
Bonini, F., Piletsky, S., Turner, A.P.F., Speghini, A., Bossi, A., 2007. Biosens. Bioelectron. 22 (9), 2322–2328.
Cai, S., Zhang, Y.X., Han, K., Ding, Y.Q., 2017. Arch. Gynecol. Obstet. 1–6.
Canfarotta, F., Poma, A., Guerreiro, A., Piletsky, S., 2016. Nat. Protoc. 11 (3), 443–455.
Chen, L., Xu, S., Li, J., 2011. Chem. Soc. Rev. 40 (5), 2922–2942.
Damhorst, G.L., Smith, C.E., Salm, E.M., Sobieraj, M.M., Ni, H., Kong, H., Bashir, R., 2013. Biomed. Microdevices 15 (5), 895–905.
Dewey, R.E., Timothy, D.H., Levings, C.S., 1987. Proc. Natl. Acad. Sci. 84 (15), 5374–5378.
Elshafey, R., Tavares, A.C., Siaj, M., Zourob, M., 2013a. Biosens. Bioelectron. 50, 143–149.
Elshafey, R., Tlili, C., Abulrob, A., Tavares, A.C., Zourob, M., 2013b. Biosens. Bioelectron. 39 (1), 220–225.
Frasconi, M., Mazzei, F., Ferri, T., 2010. Anal. Bioanal. Chem. 398 (4), 1545–1564.
Freeman, R., Girsh, J., Fang-ju Jou, A., Ho, J.-aA., Hug, T., Dernedde, J., Willner, I., 2012. Anal. Chem. 84 (14), 6192–6198.
Fu, X.-M., Liu, Z.-J., Cai, S.-X., Zhao, Y.-P., Wu, D.-Z., Li, C.-Y., Chen, J.-H., 2016a. Chin. Chem. Lett. 27 (6), 920–926.
Fu, X.M., Liu, Z.J., Cai, S.X., Zhao, Y.P., Wu, D.Z., Li, C.Y., Chen, J.H., 2016b. Chin. Chem. Lett. 27 (6), 920–926.
Gaafar, R., Bahnassy, A., Abdelsalam, I., Kamel, M.M., Helal, A., Abdel-Hamid, A., Eldin, N.A., Mokhtar, N., 2010. Lung Cancer 70 (1), 43–50.
Gao, J., Liu, W., Xia, Y., Li, W., Sun, J., Chen, H., Li, B., Zhang, D., Qian, W., Meng, Y., Deng, L., Wang, H., Chen, J., Guo, Y., 2011. Biomaterials 32 (13), 3459–3470.
Hashida, S., Ishikawa, E., 1985. Anal. Lett. 18 (9), 1143–1155.
Han, J., Go, G., Zhen, J., Zheng, S., Le, V.H., Park, J.-O., Park, S., 2017. Sens. Actuators B: Chem. 240, 1226–1236.
Herrlinger, U., Wiendl, H., Renninger, M., Förschler, H., Dichgans, J., Weller, M., 2004. Br. J. Cancer 91 (2), 219–224.
Hudelist, G., Köstler, W.J., Gschwantler-Kaulich, D., Czerwenka, K., Kubista, E., Müller, R., Helmy, S., Manavi, M., Zielinski, C.C., Singer, C.F., 2006. Eur. J. Cancer 42 (2), 186–192.
Ilkhani, H., Sarparast, M., Noori, A., Bathaie, S.Z., Mousavi, M.F., 2015. Biosens. Bioelectron. 74, 491–497.
Ilyas, A., Asghar, W., Allen, P.B., Duhon, H., Ellington, A.D., Iqbal, S.M., 2012. Nanotechnology 23 (27), 275502–275509.
Jagner, D., 1982. A review. Analyst 107 (1275), 593–599.
Johari-Ahar, M., Rashidi, M., Barar, J., Aghaie, M., Mohammadnejad, D., Ramazani, A., Karami, P., Coukos, G., Omidi, Y., 2015. Nanoscale 7 (8), 3768–3779.
Karami, P., Majidi, M.R., Johari-Ahar, M., Barar, J., Omidi, Y., 2017. Biosens. Bioelectron. 92, 287–293.
Kim, M.-J., Lee, H.J., Lee, I.-A., Kim, I.-Y., Lim, S.-K., Cho, H.-A., Kim, J.-S., 2008. Arch. Pharmacal Res. 31 (4), 539.
Kim, Y.-I., Jeong, S., Jung, K.O., Song, M.G., Lee, C.-H., Chung, S.-J., Park, J.Y., Cha, M.G., Lee, S.G., Jun, B.-H., 2017. Sci. Rep. 7.
Kryscio, D.R., Peppas, N.A., 2012. Acta Biomater. 8 (2), 461–473.
La Pera, L., Lo Curto, S., Visco, A., La Torre, L., Dugo, G., 2002. J. Agric. Food Chem. 50 (11), 3090–3093.
Lee, H.S., Kim, K.S., Kim, C.J., Hahn, S.K., Jo, M.H., 2009. Biosens. Bioelectron. 24 (6), 1801–1805.
Li, R., Huang, H., Huang, L., Lin, Z., Guo, L., Qiu, B., Chen, G., 2013a. Electrochim. Acta 109, 233–237.
Li, R., Huang, H., Huang, L., Lin, Z., Guo, L., Qiu, B., Chen, G., 2013b. Electrochim. Acta 109, 233–237.
Liu, F., Zhang, J., Deng, Y., Wang, D., Lu, Y., Yu, X., 2011. Sens. Actuators, B: Chem. 153 (2), 398–403.
Ludwig, J.A., Weinstein, J.N., 2005. Nat. Rev. Cancer 5 (11), 845–856.
Lv, Z., Wang, K., Zhang, X., 2014. J. Immunoass. Immunochem. 35 (3), 233–240.
Majidi, M.R., Omidi, Y., Karami, P., Johari-Ahar, M., 2016. Talanta 150, 425–433.
Moreira, F.T.C., Dutra, R.A.F., Noronha, J.P.C., Fernandes, J.C.S., Sales, M.G.F., 2013. Sens. Actuators B: Chem. 182, 733–740.
Moreira, F.T.C., Ferreira, M.J.M.S., Puga, J.R.T., Sales, M.G.F., 2016. Sens. Actuators B: Chem. 223 (Suppl. C), S927–S935.
Mousavi, M.F., Mirsian, S., Noori, A., Ilkhani, H., Sarparast, M., Moradi, N., Bathaie, S.Z., Mehrgardi, M.A., 2017. Electroanalysis 29 (3), 861–872.
Nonaka, Y., Ikebukuro, K., 2012. Electrochemistry 80 (5), 363–366.
Omidfar, K., Darzianiazizi, M., Ahmadi, A., Daneshpour, M., Shirazi, H., 2015. Sens. Actuators B: Chem. 220, 1311–1319.
Patris, S., De Pauw, P., Vandeput, M., Huet, J., Van Antwerpen, P., Muyldermans, S., Kauffmann, J.-M., 2014. Talanta 130 (Suppl. C), S164–S170.
Phares, N., White, R.J., Plaxco, K.W., 2009. Anal. Chem. 81 (3), 1095–1100.
Punter-Villagrasa, J., del Moral-Zamora, B., Colomer-Farrarons, J., Miribel-Catala, P., Cid, J., Rodriguez-Villarreal, I., Prieto-Simon, B., 2014. Proceedings of the 2014 11th International Multi-Conference on Systems, Signals & Devices (SSD), IEEE, pp. 1–6.
Qureshi, A., Gurbuz, Y., Niazi, J.H., 2015. Sens. Actuators B: Chem. 209, 645–651.
Ravalli, A., Rivas, L., De La Escosura-Muñiz, A., Pons, J., Merkoçi, A., Marrazza, G., 2015. J. Nanosci. Nanotechnol. 15 (5), 3411–3416.
Regiart, M., Fernández-Baldo, M.A., Villarroel-Rocha, J., Messina, G.A., Bertolino, F.A., Sapag, K., Timperman, A.T., Raba, J., 2017. Anal. Chim. Acta 963, 83–92.
Ren, D., Xia, Y., Wang, B., You, Z., 2016. Anal. Chem. 88 (8), 4318–4327.
Song, H., He, R., Wang, K., Ruan, J., Bao, C., Li, N., Ji, J., Cui, D., 2010. Biomaterials 31 (8), 2302–2312.
Song, X., Xu, S., Chen, L., Wei, Y., Xiong, H., 2014. J. Appl. Polym. Sci. 131 (16), 40766–40783.
Tabrizi, M.A., Shamsipur, M., Saber, R., Sarkar, S., 2017. Sens. Actuators B: Chem. 240, 1174–1181.
Takahashi, Y., Miyamoto, T., Shiku, H., Asano, R., Yasukawa, T., Kumagai, I., Matsue, T., 2009. Anal. Chem. 81 (7), 2785–2790.
Tamura, M., Ohta, Y., Nakamura, H., Oda, M., Watanabe, G., 2001. Int. J. Biol. Markers 17 (4), 275–279.
Tarley, C.R.T., Santos, V.S., Baêta, B.E.L., Pereira, A.C., Kubota, L.T., 2009. J. Hazard. Mater. 169 (1), 256–262.
Tian, T., Liu, H., Li, L., Yu, J., Ge, S., Song, X., Yan, M., 2017. Sensors and Actuators. B: Chem. 251, 440–445.
Tjalma, J.J., Garcia-Allende, P.B., Hartmans, E., van Scheltinga, A.G.T., Boersma-van Ek, W., Glatz, J., Koch, M., van Herwaarden, Y.J., Bisseling, T.M., Nagtegaal, I.D., 2016. J. Nucl. Med. 57 (3), 480–485.
Tüdős, A.J., Besselink, G.A., Schasfoort, R.B., 2001. Lab Chip 1 (2), 83–95.
Vasudev, A., Kaushik, A., Bhansali, S., 2013. Biosens. Bioelectron. 39 (1), 300–305.
Wan, Y., Liu, Y., Allen, P.B., Asghar, W., Mahmood, M.A.I., Tan, J., Duhon, H., Kim, Y.T., Ellington, A.D., Iqbal, S.M., 2012. Lab Chip - Miniat. Chem. Biol. 12 (22), 4693–4701.
Wang, L., Zheng, Q., Zhang, Q., Xu, H., Tong, J., Zhu, C., Wan, Y., 2012. Oncol. Lett. 4 (5), 935–940.
Wegner, K.D., Lindén, S., Jin, Z., Jennings, T.L., Khoulati, Re, van Bergen en Henegouwen, P.M., Hildebrandt, N., 2014. Small 10 (4), 734–740.
Yuan, Z., Lu, F., Peng, M., Wang, C.-W., Tseng, Y.-T., Du, Y., Cai, N., Lien, C.-W., Chang, H.-T., He, Y., 2015. Anal. Chem. 87 (14), 7267–7273.
Zhao, S., Yang, W., Lai, R.Y., 2011. Biosens. Bioelectron. 26 (5), 2442–2447.
Zhou, W., Bai, M., Jin, Y., 2009. Int. J. Tuberc. Lung Dis. 13 (3), 381–386.